European Rotorcraft Forum

DESIGN AND TESTING OF AN ACTIVE VIBRATION ABSORBER FOR A HELICOPTER ROTOR

Giovanni Bianchi* (1), Michele Zilletti (2), Fabio De Giorgio (1), Simone Cinquemani (1), Gabriele Cazzulani (1), Ermanno Fosco (2), Luigi Bottasso (2), Francesco Braghin (1)

*giovanni.bianchi@polimi.it ,

[b] michele.zilletti@leonardo.it

(1) Politecnico di Milano, Dipartimento di Meccanica, Via La Masa 1, 20156, Milano (Italy)

(2) Leonardo Helicopters, Via Giovanni Agusta, 520, 21017 Samarate VA (Italy)

Abstract

This article presents the design and the experimental tests on a prototype of an active vibration absorber for helicopter rotors. The main disturbance forces are those transferred by the blades to the rotor, which are harmonic with a frequency multiple of the rotor angular speed times the number of blades, and the device aims to counteract the two main frequencies of the disturbance. This device is composed of two identical subsystems, one for each frequency, which are put in rotation by a mechanical transmission connected to the rotor hub guaranteeing that the generated force always has the correct frequency for any angular velocity of the rotor. On each subsystem, there are two eccentric masses actuated by electric motors, which are used to modulate the amplitude and the phase of the generated force. The control algorithm of the device is based on the EPLL harmonic tracking to identify the amplitude and the phase of the disturbance, and the positioning algorithm allows to place the masses in the correct position avoiding collisions between them. The device has been built and tested on a dedicated test bench, measuring the generated forces. The results of the experiments are promising since the eccentric masses follow the reference positions, indicating that the device would significantly suppress the vibrations.

1. INTRODUCTION

Despite significant research efforts and many technological solutions developed over the last four decades, vibration reduction remains high on the agenda of the rotorcraft industry. Rotors and drive trains generate vibrations in the range of acoustic and dynamic discomfort for humans. Furthermore, vibrations have a detrimental effect on the reliability of helicopter systems and avionics equipment and affect the fatigue life of structures. Therefore, excessive vibration remains both a challenging and an urgent problem to address.

This work is focused on the development of an active vibration absorber for the main rotor of a helicopter to reduce the vibration at the source, thus also inside the cabin and improve crew and passengers' comfort. The paper describes the design of the vibration absorber prototype and laboratory test to assess its main functionalities.

Among different vibration sources, the oscillating loads transferred from the blades to the rotor hub, whose frequencies are multiples of the rotor angular speed, are the most relevant. The rotor acts as a mechanical filter; thus, the total force $\boldsymbol{F(t)}$ transferred to the hub can be written as the sum of components having frequencies multiple of the angular speed times the number of blades:

$$\boldsymbol{F(t) = \sum_{n=-\infty}^{+\infty} F_n \cos(nb\,\Omega t + \phi_n)} \qquad (1)$$

where $\boldsymbol{b}$ is the number of blades, $\boldsymbol{\Omega}$ is the rotor angular speed, and $\boldsymbol{F_n}$ and $\boldsymbol{\phi_n}$ are the modulus and phase of the n-th harmonic component. The first-order component (at the blade passing frequency) is usually the dominant one, while the higher-order harmonic amplitudes decrease with the frequency. This suggests that a significant vibration reduction can be achieved with a dynamic vibration absorber designed to counteract the first component. In general, in a helicopter, most vibratory energy is transmitted in the frequency band 1-50 Hz.

The proposed device is designed for a five-bladed main rotor; thus, the harmonic force components to counteract are:

$$f_{+1}(t) = F_{+1}\cos(+5\Omega t + \phi_{+1}),$$

Presented at 48th European Rotorcraft Forum, Winterthur, Switzerland, 6-9 September, 2022

$$f_{-1}(t) = F_{-1}\, cos(-5\Omega t + \phi_{-1}),$$

For a given Ω, the amplitudes, F_{+1} and F_{-1}, and phases, ϕ_{+1} and ϕ_{-1}, may vary during operations. Thus, the active vibration absorber shall follow these changes and generate the two necessary counterbalancing forces in real-time.

Considering the intrinsic nature of vibration in rotary wing aircraft design, a series of different attenuation strategies have been implemented using passive or active devices over the years. The main advantage of active systems is frequency tuning, allowing the targeting and compensation of external forces with high precision and, most importantly, in a wide variety of operating conditions i.e., also when the disturbance is subject to frequency drifts.

1.1. State of the art

One control strategy implemented for vibration suppression is Higher Harmonic Control (HHC), with actuators in the fixed reference frame acting directly on the swash plate. A very similar concept is the Individual Blade Control (IBC) with actuators in the rotating reference frame acting on each individual blade. For both, a set of sensors installed on the fuselage measure the accelerations, which are subsequently elaborated with an accurate dynamic model of the helicopter to find the control inputs to apply on the blades [1] [2].

A different strategy is to employ the Harmonic Force Generator, developed by Sikorsky, which exploits the centrifugal force provided by a concentrated mass placed on the edge of a rotating disc, constrained to an arm actuated by an external source. Since the disc radius is precisely half of the circular guide radius, the mass moves on a linear trajectory. The force generated can be adjusted in phase by the actuator, while the amplitude of the sinusoidal force remains constant, as it depends on its rotational speed matching the frequency of the harmonics to be canceled. Two devices are needed to effectively suppress in-plane vibrations, one for each axis [3].

Another active device is the Active Pendulum Vibration absorber designed by Airbus. This device is, in principle, equal to a passive pendulum TMD (Tuned Mass Damper) connected to the rotor hub with springs. The active component of the device consists of a secondary mass able to move along the pendulum to modify the natural frequency [4].

A different device is Dual Frequency Hub-Mounted Vibration Suppressor developed by Sikorsky. This device is installed on the rotor hub and controls the amplitude and phase of the centrifugal forces generated by moving masses. These masses are composed of two-wheeled trucks, constrained on annular rails linked to the rotor hub, and interact with electromagnets. The information about the instantaneous angular position of each mass is not acquired by encoders, but rather an influence coefficient method is implemented, requiring a real-time estimation of the unbalancing force to compute the position of the mass. The main advantage of this device is a reduced overall added weight and a compact design [5] [6] [7].

A similar device is the Circular Force Generator adopted by the Lord Corporation. It shares the main characteristics of most Active Vibration Absorbers, utilizing eccentric masses to generate a force output that is correctly modulated in amplitude and phase. One mass is called master and connected to the device chassis, while the second is called slave and is connected directly to the master mass. The control logic utilizes two different actuators, one for the master mass, which dictates the harmonic frequency of the desired counteracting force, and the other one commands the relative movement of the two masses, effectively modifying the amplitude and phase of the overall output force [8].

The Rotor Hub Vibration Attenuator, developed by Textron Innovation, is installed on the main rotor hub. The counteracting force is obtained by rotating a set of disk-like components with asymmetric mass distribution. By correctly controlling the angular position of the masses, it is possible to modulate the amplitude and phase of the counteracting force. The control logic implemented in these systems uses both a feedback loop, closed by opportunely placed accelerometers, and a feedforward component generated by the operational parameters of the aircraft, such as blades pitch angle, generated thrust, forward velocity, and other avionics data. The two configurations are compatible with multiple Vibration Absorber devices, perpendicular or coaxial to the rotor axis [9].

The vibration suppression device presented in this article is mounted on the main rotor hub of the helicopter, and it suppresses vibrations thanks to the centrifugal forces generated by rotating eccentric masses [10]. The main innovation of this device is that the masses are put in rotation at the desired speed by a mechanical transmission connected to the rotor hub, and the motors of the device are used only to modulate the amplitude and the phase of the generated force. This ensures that the generated force always has the correct frequency for any angular velocity of the rotor. Moreover, it has the advantage of taking the most power from the rotor, minimizing the size of the motors installed on the device, and reducing the overall system's dimensions, allowing installing the device under the beanie. In addition, the control algorithm developed for this device is based on the enhanced phase-locked loop (EPLL), representing a complete novelty

Presented at 48th European Rotorcraft Forum, Winterthur, Switzerland, 6-8 September 2022

in the field of vibration control of mechanical systems.

In Section 2, the conceptual design of the device is described, and its working principle is presented; in Section 3, the control algorithm is explained, and in Section 4, the experimental results obtained on a dedicated test bench are presented and commented on. Finally, Section 5 is dedicated to the conclusions.

2. CONCEPTUAL DESIGN

This active mast vibration absorber (AMVA) is designed to address the two main harmonics of the disturbance, i.e., $+\mathbf{5\Omega}$ and $-\mathbf{5\Omega}$. Hence, the device is composed of two independent subsystems, one for each targeted harmonic. The counteracting force in each subsystem is obtained by exploiting the centrifugal forces provided by two coplanar eccentrical masses. The reason why using two masses relies on the characteristic of the disturbance forces: the amplitude of the harmonics under scope can assume a wide range of values and fluctuate over time, requiring each subsystem to adapt to these variations. Utilizing two masses, each subsystem has 2 DoFs, and each mass $\boldsymbol{i}$ generates a centrifugal force equal to:

$$\vec{F}_i = m\,(5\Omega)^2 b\,\vec{\imath}_i \qquad (3)$$

The resultant centrifugal force can be calculated by a simple vector sum. Hence, it is possible to modulate the amplitude of the resulting force of one exciter by adjusting the relative angle between the two masses and its phase by shifting both masses of the same angle.

Figure 1 shows a conceptual scheme of the proposed active vibration absorber, which consists of two sub-systems: the upper exciter (marked in green) used to generate the $\boldsymbol{f_{-1}(t)}$ component and the lower exciter (marked in red) used to generate $\boldsymbol{f_{+1}(t)}$ component.

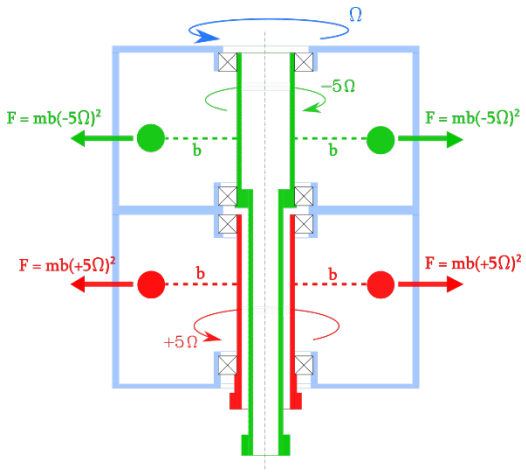

Figure 1 - Conceptual scheme of the active vibration absorber showing the upper (green) and lower (red) exciters, each consisting of two eccentric masses.

In practice, the rotation of the masses can be seen as the superposition of two different motions:

- a principal motion at a speed of $+5\Omega$ or -5Ω for the lower and upper exciter respectively generated by a mechanical transmission which connects the two exciters to the main rotor hub and to a stationary point in the helicopter main gearbox. This solution ensures automatic synchronization and thus self-tuning of the exciters, warranting optimal effectiveness even when rotor rpms change.

- a corrective motion, used to adjust the position of the masses in the rotating reference frame, modulate amplitude and phase of the resulting force, produced by four independent electric motors, one for each mass.

As mentioned earlier, the adoption of a gearbox ensures that the principal motion is synchronous with the actual rotor angular speed even in the case of angular speed variations that may occur during flight. Thus, the force generated by the device has always the correct frequency. Another advantage is that the required power for this motion is taken directly from the mast without the need for a separate power source (e.g., an electric motor).

Conversely, the corrective motion is independent of the rotation of the helicopter rotor, and it shall be executed as swiftly as possible to be able to follow in real-time the modulus and phase variations of the primary excitation.
The coaxial mounting of shafts and the subsystem planes being as close as feasible are choices made to save space and minimize the moments.

Presented at 48th European Rotorcraft Forum, Winterthur, Switzerland, 6-8 September 2022

The masses are free to move radially, so they are pushed against the external case, decreasing the loads acting on the shafts, and allowing the subsystems to have a more compact size. The two subsystems are completely independent of each other and have all the required actuators and sensors on board, rising the reliability of the overall system. The only common links the two subsystems have are the connection to the same mechanical transmission and the powerline needed for the control algorithm and the actuators.

Therefore, each subsystem is equipped with:

- a slip ring to transmit power and signal to the rotating reference frame;
- an electronic board;
- two geared brushless motors with their electronic drives and their encoders;
- two proximity sensors to initialize the masses positions in the rotating reference frame;
- one proximity sensor to initialize the position of the $\pm 5\Omega$ reference frame with respect to the Ω reference frame.

To reduce the total height of each subsystem, the motors that move the masses are not mounted coaxially with the main shafts, but they are mounted at a radial distance from the shaft axis, and the masses are actuated through a system of concentric gears, as shown in Figure 2.

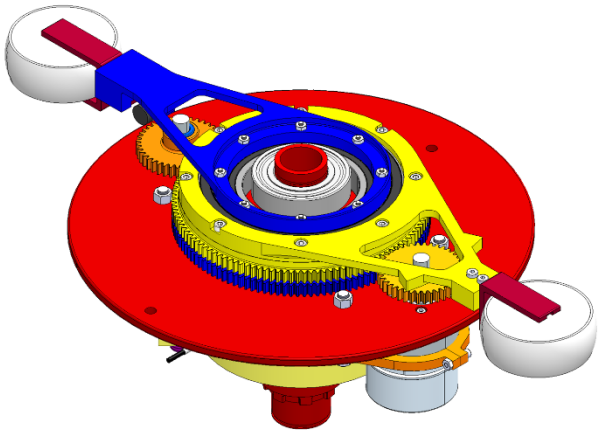

Figure 2 - +5Ω subsystem showing the system of gears that transmits the motion from the motor to the masses

3. CONTROL ALGORITHM

In order to obtain the desired counteracting forces from the two subsystems, the control algorithm follows the block diagram shown in Figure 3:

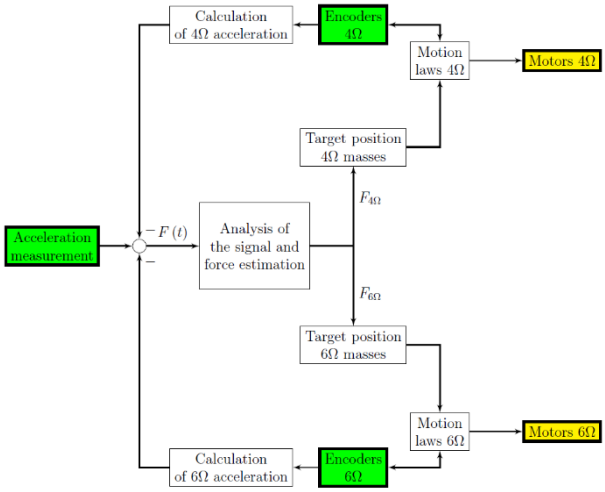

Figure 3 - Block diagram of the control algorithm

To ensure the correct positioning of the masses during operation, the following steps are required:

1. measurement of the acceleration at the rotor hub;
2. based on the measured acceleration signal acquired at step 1, estimation of the instantaneous amplitudes f_1^+ and f_1^- and phases, ϕ_1^+ and ϕ_1^-, of the external force which is needed to counterbalance the disturbance;
3. calculation of the target positions of each mass;
4. based on the encoder reading of the actual position of masses, calculation of the motion law for each motor;
5. communication of the information to the motors;
6. motion of the masses from the current to the target position;
7. knowing the position of the masses from the signal of the encoder, calculation of the effect of each exciter on the system. The force that must be counteracted is only the disturbance force coming from the blades, whereas the measured signal is the sum of the effect of the disturbance force and the force generated by the exciters. Hence, it is necessary to subtract the effect of the exciters from the measured acceleration signal.

As the amplitude and phase of the external forces continuously change in a realistic operational scenario, the steps described above need to be executed with an acceptable level of readiness. This defines stringent requirements on the signal processing algorithm for steps 2, 3, and 4 and the response of the positioning motors at step 5 to avoid unwanted delays.

3.1. Force estimation

The estimation of the force vector, in step 2, is carried out using a harmonic identification technique based

Presented at 48th European Rotorcraft Forum, Winterthur, Switzerland, 6-8 September 2022

on the Enhanced-Phase-Locked-Loop (EPLL). EPLL is a non-linear adaptive band-pass filter capable of tracking a sinusoidal signal and detecting frequency variations [11]. The EPLL is commonly used in electric grids management [12], and its use in the control of mechanical vibrations represents a complete novelty. To adapt the behavior of the filter to the specific application it is required to fine-tune three gains following the methods described in the literature [11] [12]. Tuning the gains, it is possible to shape the transient behavior of the EPLL, and the more this system is prompt to react to changes of amplitude or phase, the less it can cancel out the noise present in the signal. Therefore, the gains were tuned to have the same transient time of estimation as the transient time of the actuation. In this way, all the signal variations that the motors can follow are correctly estimated by the algorithm, whereas all the variations with dynamics faster than the motor's dynamics are canceled out together with the noise.

3.2. Positioning algorithm

For each subsystem $\boldsymbol{i}$, once the amplitude $\boldsymbol{U_i}$ and the phase $\boldsymbol{\phi_i}$ of each force vector are known, the positioning algorithm computes the masses' positions that generate the required counteracting force. The first step consists in calculating the relative angle between the two masses:

$$\Delta\theta = \cos^{-1}\left(\frac{U_i}{2\,m\,(5\Omega)^2 r}\right) \tag{4}$$

Utilizing the estimated phase $\boldsymbol{\phi_i}$ from the EPLL, the final target positions are:

$$\theta_{1,2} = \phi_i + \pi \pm \Delta\theta \tag{5}$$

Then, it is necessary to correctly lead the two masses into these positions, considering that:

- the masses are susceptible to collisions since they are coplanar;
- multiple paths are available, being the angular position a periodic value;
- the total traveled distance must be minimized.

It is always possible to reach both targets with a rise $0 < |h| < \pi$; therefore, only the shortest path from point A to point B will be selected by the algorithm.

Let us define a pair of rises (h_A, h_B), with the constraint that these rises are relative to the starting masses positions θ_A and θ_B going into two different target positions, θ_1 and θ_2.

Let us also define the total rise $Hi = h_A + h_B$ of said pair. A pair of rises is considered feasible if it prevents the collision between the masses, while the total rise is an indicator of the required time to reach the desired destinations.

Without any loss of generality, in the following demonstration some assumptions are made:

- $\theta_B = 0$
- $\theta_A > 0;\ \theta_1, \theta_2 < 2\pi$
- $\theta_2 > \theta_1$
- $\theta_2 - \theta_1 \leq \pi$

These assumptions are always valid if a proper choice of $\theta_A, \theta_B, \theta_1, \theta_2$ is taken.

Given these hypotheses, five scenarios are possible:

- **Case 1**: $\theta_A > \theta_2\ ;\ \theta_A < \pi$

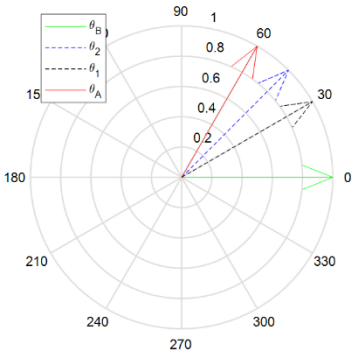

$$\begin{cases} H\binom{A \to 1}{B \to 2} = H_1 = (\theta_A - \theta_1) + \theta_2 \\ H\binom{A \to 2}{B \to 1} = H_2 = (\theta_A - \theta_2) + \theta_1 \\ H_1 - H_2 = 2(\theta_2 - \theta_1) > 0 \end{cases} \tag{5}$$

H_1 is not feasible, H_2 is feasible, $H_2 < H_1$

- **Case 2**: $\theta_2 > \theta_A > \theta_1\ ;\ \theta_2 < \pi$

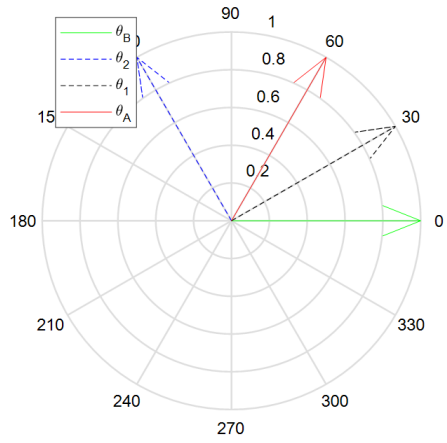

$$\begin{cases} H\binom{A \to 1}{B \to 2} = H_1 = (\theta_A - \theta_1) + \theta_2 \\ H\binom{A \to 2}{B \to 1} = H_2 = (\theta_2 - \theta_A) + \theta_1 \\ H_1 - H_2 = 2(\theta_A - \theta_1) > 0 \end{cases} \tag{6}$$

H_1 is not feasible, H_2 is feasible, $H_2 < H_1$

- **Case 3**: $\theta_2 > \theta_1 > \theta_A\ ;\ \theta_2 < \pi$

Presented at 48th European Rotorcraft Forum, Winterthur, Switzerland, 6-8 September 2022

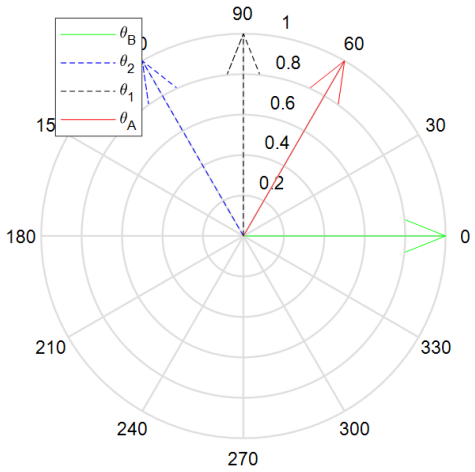

$$\begin{cases} H\begin{pmatrix} A & \to 1 \\ B & \to 2 \end{pmatrix} = H_1 = (\theta_1 - \theta_A) + \theta_2 \\ H\begin{pmatrix} A & \to 2 \\ B & \to 1 \end{pmatrix} = H_2 = (\theta_2 - \theta_A) + \theta_1 \\ H_1 - H_2 = 0 \end{cases} \quad (7)$$

$H_1$is not feasible, $H_2$is feasible, $H_2 = H_1$

- **Case 4**: $\pi < \theta_2 < \theta_A + \pi$; $\theta_A < \theta_1 < \pi$

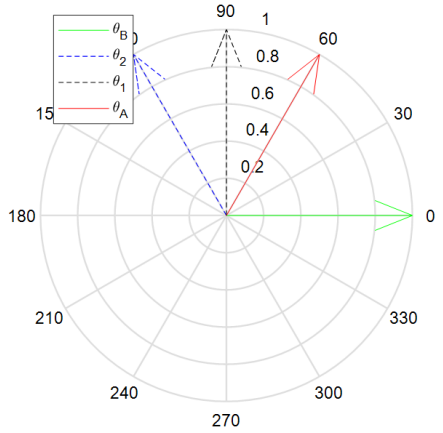

$$\begin{cases} H\begin{pmatrix} A & \to 1 \\ B & \to 2 \end{pmatrix} = H_1 = (\theta_1 - \theta_A) + (2\pi - \theta_2) \\ H\begin{pmatrix} A & \to 2 \\ B & \to 1 \end{pmatrix} = H_2 = (\theta_2 - \theta_A) + \theta_1 \\ H_1 - H_2 = 2(\pi - \theta_2) \end{cases} \quad (8)$$

$H_1$is feasible, $H_2$is feasible, $H_2 > H_1$

- **Case 5**: $\theta_2 > \theta_A + \pi$; $\theta_A < \theta_1 < \pi$

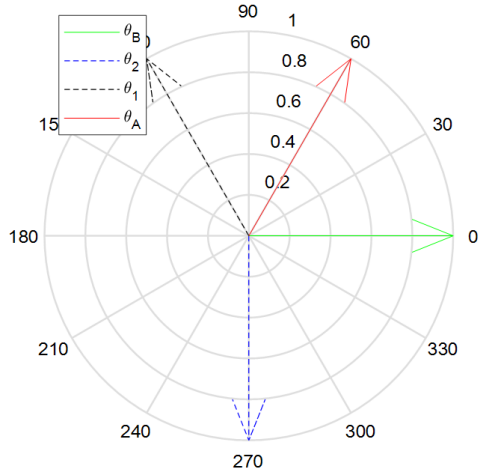

$$\begin{cases} H\begin{pmatrix} A & \to 1 \\ B & \to 2 \end{pmatrix} = H_1 = (\theta_1 - \theta_A) + (2\pi - \theta_2) \\ H\begin{pmatrix} A & \to 2 \\ B & \to 1 \end{pmatrix} = H_2 = (2\pi - \theta_2 + \theta_A) + \theta_1 \\ H_1 - H_2 = -2\,\theta_A < 0 \end{cases} \quad (9)$$

$H_1$is feasible, $H_2$is not feasible, $H_2 > H_1$

It can be observed that for any possible set of initial and final angular positions, a feasible rise exists, and it is such to minimize the total displacement. This result implies that minimizing the total displacement ensures avoiding collisions. The only exception is Case 3, where both paths H_1 and H_2 have the same value. However, sorting the mass positions and target positions, and keeping the same order (higher mass position ⇒ higher target position) when assigning the rises is enough to guarantee any collision from happening.

3.3. Communication with motors

The motors used for this device are Maxon EC flat motors, commanded with their drives EPOS2 integrated into the electronic board. The target positions are communicated through serial RS232 communication, and the minimum interval between two consecutive messages is 36 ms. The motors follow a trapezoidal motion law, and its correct execution is guaranteed by an internal PID control of the drives.

3.4. Position measurement

The angular position of the masses is initialized at the beginning of the test when they pass in correspondence with the proximity sensors. Then, an incremental encoder embedded with the motors measures the angular displacement, and the current position of the masses can be calculated considering

Presented at 48th European Rotorcraft Forum, Winterthur, Switzerland, 6-8 September 2022

the transmission ratio of the gears.

4. EXPERIMENTAL TESTS

The scope of the experimental tests carried out on a dedicated test bench shown in Figure 4 is to evaluate the absorber's capability to generate suitable control forces when a realistic reference signal is fed to the controller. Thus, the acceleration signal is stored in the boards' memory and the balancing force is generated and measured. Finally, during post-processing, the force measurements are compared with the original signal. In a real helicopter application, an estimate of the acceleration to force transfer function would be required. In this case, to characterize the absorber dynamics, the rig has been designed to ground the device and measure the blocked force. Therefore, the signal given as a reference is not acceleration but force.

4.1. Test bench

Each of these pulleys is connected with a toothed belt to a pulley mounted on one of the two shafts or the external case. The pulley at the bottom has a transmission ratio of $-3/2$ and it is connected to the -5Ω shaft, the pulley in the middle has a transmission ratio of $+3/2$ and is connected to the $+5\Omega$ shaft, and the pulley at the top has a transmission ratio of $3/10$, and it is connected to the external case.

The exciter assembly and the pulley system are suspended on six load cells that measure the forces and moments generated in all principal directions. The load cells are designed to be stiff enough to avoid dynamic interaction in the frequency band of interest and measure the blocked force produced by the exciters. To verify that the dynamic behavior of the test bench does not influence the forces measurements, some significant frequency response functions of the system have been calculated. These tests have been performed by exciting the system with an impact hammer creating a force in the radial direction in the plane of the masses and measuring

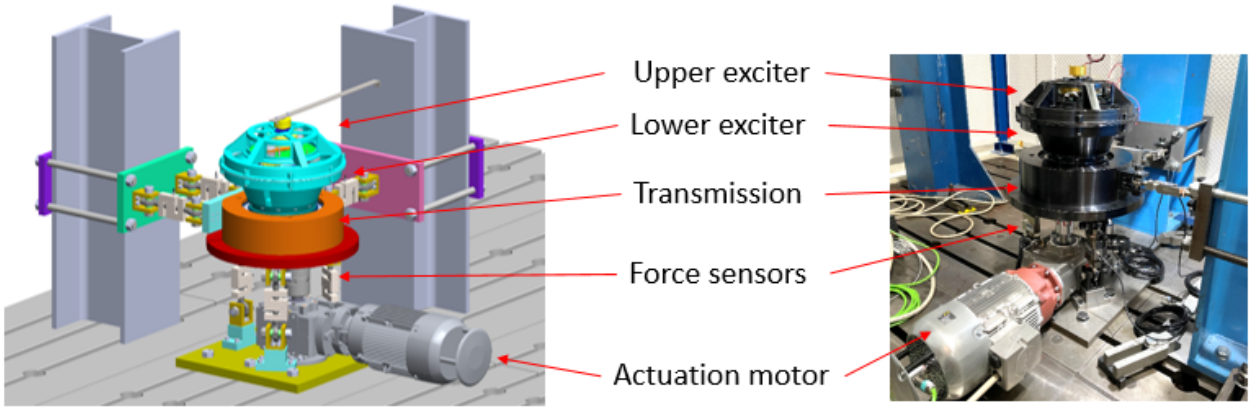

Figure 4 – test bench: CAD model (left), experimental setup (right)

The actuation motor is an asynchronous electric motor Siemens 1FT7082, with a nominal power of 4 kW. It is connected to a bevel gear transmission, and the output of this transmission is connected with a flexible joint to a shaft with three pulleys, which rotates at $^{10}/_{3}\,\Omega$, as shown in Figure 5.

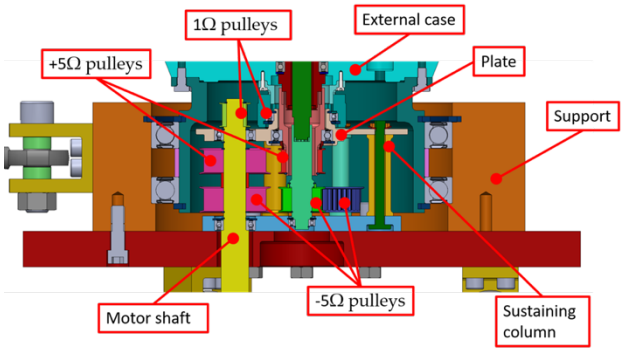

Figure 5 - Section view of the test bench pulley system

the acceleration in all three directions on the exciters and on the base. In Figure 6, the FRF of the acceleration on the exciters measured in the same position and the same direction of the force is shown. A prominent low damped peak at 1505 Hz can be noticed, followed by another peak around 2580 Hz.

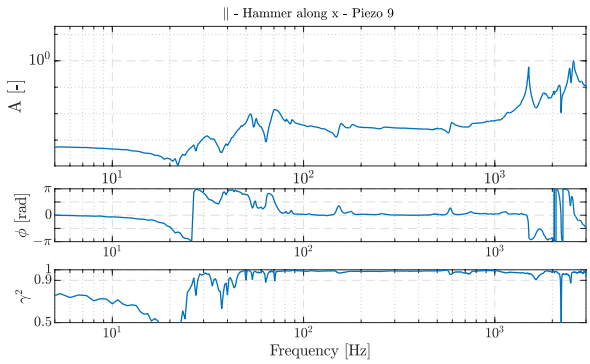

Figure 6 - FRF of the acceleration measured in the masses plane to a force applied in the same position and direction

Presented at 48th European Rotorcraft Forum, Winterthur, Switzerland, 6-8 September 2022

There are also some less pronounced peaks in the lower frequencies. However, the dimensionless damping correlated to those peaks is higher, as shown in Table 1, and they are not a cause of concern.

Table 1 - Adimensional damping of the vibration modes of the exciters

32 Hz	h = 7.4 %
52 Hz	h = 2.7 %
71 Hz	h = 4.1 %
157 Hz	h = 4.3 %
1507 Hz	h = 0.34 %

4.2. Experimental results

During these tests, the aMVA is treated as a feedforward system, elaborating in real-time a force time history preloaded on the electronic board. These time histories can be classified into two main categories:

- Synthetic signals: they are artificial noiseless force disturbance histories with step-like variations of amplitude and phase, as the one shown in Figure 7. They are aimed at characterizing the exciters and debugging the software.

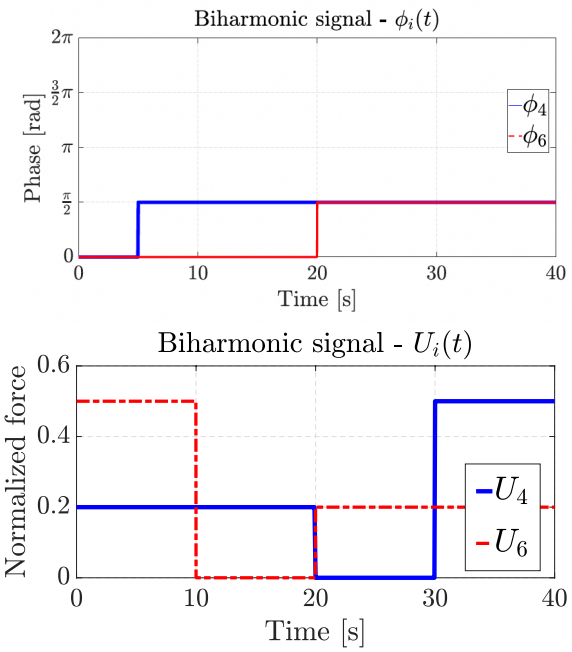

Figure 7 - Amplitude and phase of the biharmonic synthetic signal

- Real measurement signals: they are derived from past analyses performed by Leonardo Helicopters in different operative conditions, as the one shown in Figure 8.

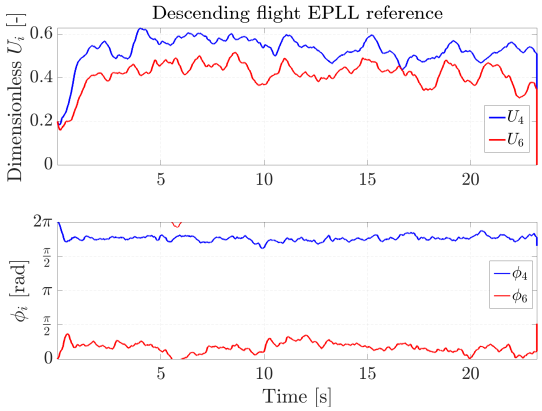

Figure 8 - Estimated amplitude and phase of the time history of a real flight

The forces are measured by the load cells fixed on the ground, so they refer to a fixed reference frame, where all forces have frequency 5Ω. Nevertheless, the reference signals refer to a rotating reference frame fixed on the rotor, rotating at 1Ω, where the forces have frequencies $+4\Omega$ and -6Ω. Therefore, it is necessary to perform a transformation of reference frames before comparing the signals. This can be done by expressing the force vector as a complex number $\bar{F}$, the subscript $n\Omega$ indicates the angular speed of the reference frame, and the subscripts x and y represent the axis on which the force is measured:

$$\bar{F}_{0\Omega} = F_{x,0\Omega} + iF_{y,0\Omega} \tag{10}$$

The complex force in the reference frame is related to the complex force in a rotating reference frame through the following expression:

$$\bar{F}_{n\Omega} = \bar{F}_{0,\Omega} e^{-i\int_0^t n\Omega\tau\, d\tau} \tag{11}$$

Passing from the fixed reference frame to a reference frame rotating at 1Ω the measured force is transformed into a biharmonic signal that can be compared with the original signal. Moreover, it is possible to pass from the fixed reference frame to a rotating reference frame at $\pm 5\Omega$, so to have the instantaneous values of amplitude and phase of the generated force of each subsystem, which also allows reconstructing the position of the masses and assessing the performance of the actuators.

In a reference frame rotating at $\pm 5\Omega$, the force is seen as a constant summed with a harmonic at $\mp 10\Omega$, which can be deleted with a stop-band filter.

In Figure 9, the results obtained with a synthetic signal are presented. The synthetic signal was designed to be as challenging as possible, with step changes of amplitude from 0 to the maximum force

Presented at 48th European Rotorcraft Forum, Winterthur, Switzerland, 6-8 September 2022

and with step phase changes of 180°. The orange line shows the force generated by the upper and lower exciter along the x-axis in a fixed reference system. The blue line shows the reference primary excitation force components to be counteracted, which are derived from a measured acceleration signal in flight. Finally, the yellow line shows the residual error signals given by the difference between the reference and measured force.

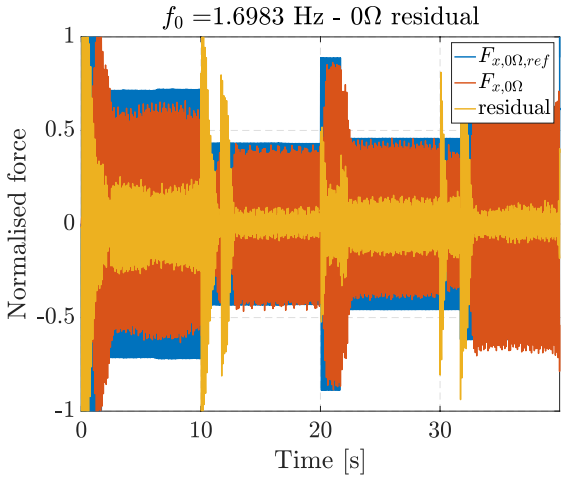

Figure 9 - Measured force in the fixed reference frame during a test with a synthetic signal

The same results are shown with respect to the reference frames rotating at $+5\Omega$ and -5Ω in Figure 10 and Figure 11. It is possible to note that after a transient lasting approximately 1.5s, the masses reach the desired positions and generate a constant force. The error with constant amplitude at the steady state is smaller than 10% of the initial amplitude, and it is due to an initializing error of masses positions. Moreover, it can be observed that the residual in the fixed reference frame has a greater amplitude than the sum of the residuals in the rotating reference frames, which occurs because the subsystems are not perfectly synchronized. Nevertheless, this issue is of minor importance because in a real flight both subsystems would receive the same signal in real-time.

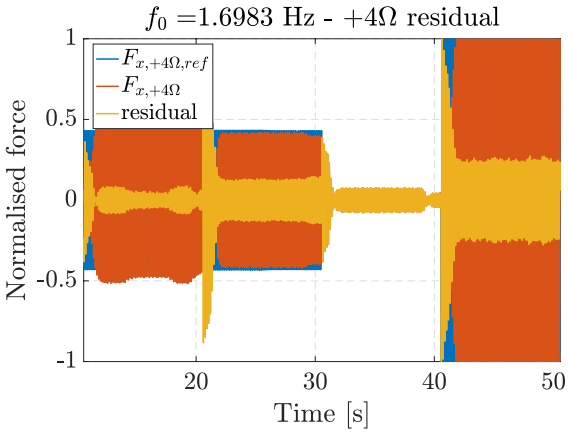

Figure 10 - Measured force of the $+5\Omega$ subsystem during a test with a synthetic signal

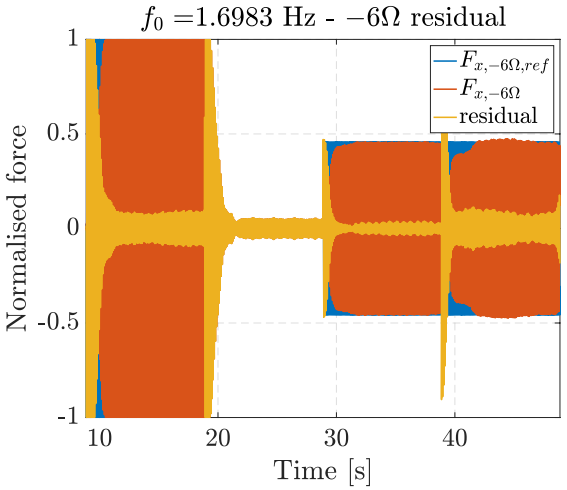

Figure 11 - Measured force of the -5Ω subsystem during a test with a synthetic signal

The instantaneous amplitude reduction is shown in Figure 12 and Figure 13.

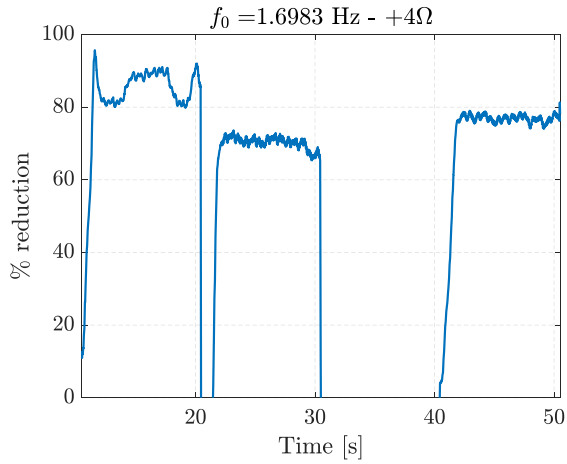

Figure 12 - Instantaneous reduction of the disturbance of the $+5\Omega$ subsystem

Presented at 48th European Rotorcraft Forum, Winterthur, Switzerland, 6-8 September 2022

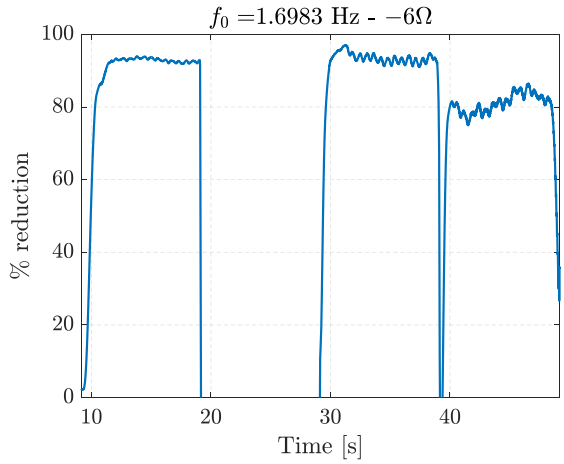

Figure 13 - Instantaneous reduction of the disturbance of the −5Ω subsystem

The same analyses can be performed with a signal measured in real flight conditions. The measured acceleration signal is transformed into a force signal simply by multiplying it with a scale factor. The instantaneous amplitude and phase of the harmonics of interest in the real flight measurement are unknown, and they have been estimated with the EPLL algorithm. Therefore, unlike for the synthetic signal for which it was possible to directly compare the original signal with the generated force, in this case, the generated force is compared with the signal estimated with the EPLL algorithm. The real flight signal has some small variations in amplitude and phase which oscillate randomly about a mean value without any sudden step change.

In Figure 14 and Figure 15 the results of the tests performed with a real signal are shown. The graphs show a comparison between the reference signal, estimated with the EPLL, the measured force in the rotating reference frame, calculated in the same way as for the synthetic signal, and the residual force, all normalized with respect to the maximum value.

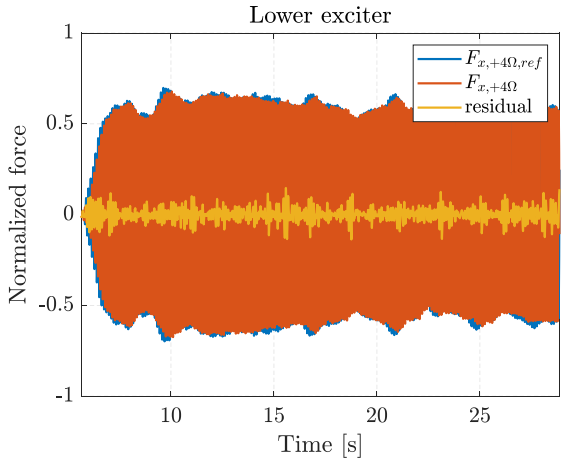

Figure 14 - Measured force of the +5Ω subsystem during a test with a real signal

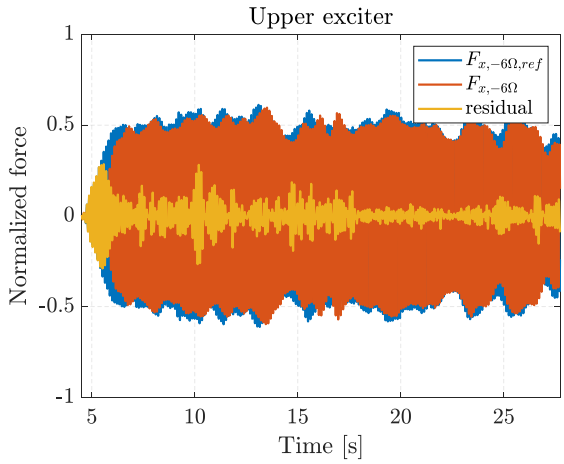

Figure 15 - Measured force of the −5Ω subsystem during a test with a real signal

This result showed that the EPLL algorithm could identify the amplitude and the phase of the harmonics of interest, motors follow the reference positions, and the eccentric masses generate a force in agreement with the reference signals with a residual force always below 25% for the lower subsystem and below 40% for the upper subsystem. The residual force is reduced to 10% of the reference force when the reference has the smallest phase variations, as displayed in Figure 16 and Figure 17.

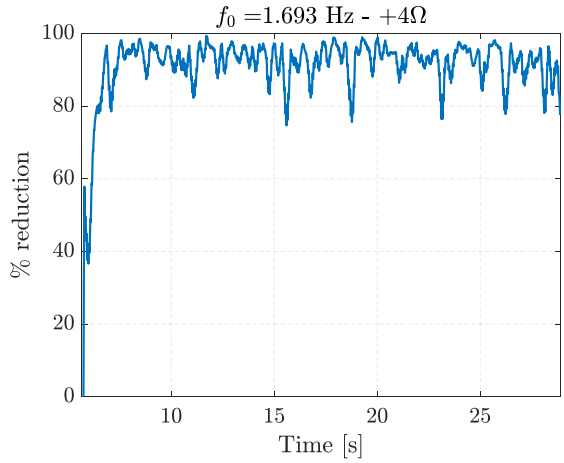

Figure 16 - Instantaneous reduction of the disturbance of the +5Ω subsystem

Presented at 48th European Rotorcraft Forum, Winterthur, Switzerland, 6-8 September 2022

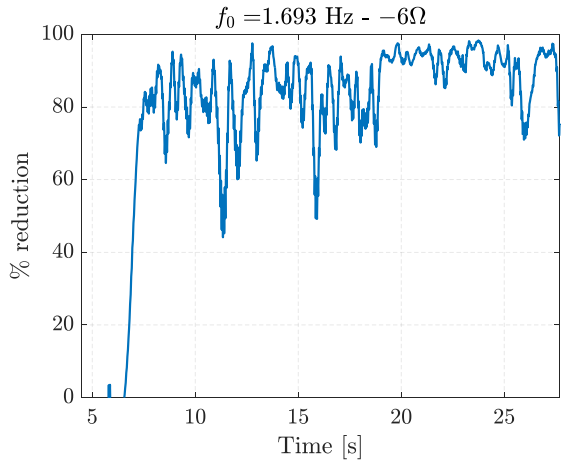

Figure 17 - Instantaneous reduction of the disturbance of the -5Ω subsystem

5. CONCLUSION

In conclusion, a prototype active vibration absorber for the helicopter rotor has been designed and built. This device generates a centrifugal force thanks to counter rotating eccentric masses, which spin at the circular frequencies to counteract, the +5Ω and the -5Ω harmonic load components. A mechanical transmission puts in rotation the two subsystems, and on each of them, two motors move the eccentric masses in the desired position to obtain the correct amplitude and phase of the forces. The disturbance forces are estimated thanks to the EPLL algorithm. The vibration absorber has been tested on a dedicated test bench, and its performances in canceling the force for a real flight time history have been evaluated. The device shows promising results, as the eccentric masses can promptly follow the reference positions, indicating that the device would significantly suppress the vibrations.

1. BIBLIOGRAPHY

[1] Q. Khanh, "Higher harmonic control analysis for vibration reduction of helicopter rotor systems.," NASA technical memorandum, 2004.

[2] D. Patt, L. Liu, J. Chandrasekar, D. Bernstein and P. Friedman, "The HHC algorithm for helicopter vibration reduction revisited," in *Structural dynamics and materials conference*, 2004.

[3] K. Frederickson.U.S.A. Patent US7958801, 2011.

[4] T. Krysinsky and M. Anthoine.U.S.A. Patent US6045090, 2000.

[5] S. Dyer.U.S.A. Patent US6618646 B1, 2003.

[6] W. Welsh.U.S.A. Patent US8403643 B2, 2013.

[7] M. Jolly and P. Black.U.S.A. Patent US8267652 B2, 2012.

[8] M. Jolly, A. Meyers and D. Mellinger.U.S.A. Patent 2012/0136533, 2012.

[9] D. Popelka and F. Stamps.U.S.A. Patent 2011/0194934, 2011.

[10] L. BOTTASSO, E. FOSCO, P. PISANI, F. VINCENZO, F. ROSA, F. BRAGHIN, G. CAZZULANI and S. CINQUEMANI, "Rotor for a hover-capable aircraft". Patent EP3766778A1, 2019.

[11] M. Kharimi-Ghartemani, "Linear and pseudolinear Enhanced Phased-Locked Loop structures," *IEEE Transactions on Industrial Electronics,* vol. 61, no. 3, pp. 1464-1474, 2014.

[12] M. Kharimi-Ghartemani, Enhanced Phased-Locked Loop Structures for Power and Energy Applications, 2014.

Presented at 48th European Rotorcraft Forum, Winterthur, Switzerland, 6-8 September 2022